Magnetic properties of amorphous $Fe_{90-x}Mn_xZr_{10}(0 \leqslant x \leqslant 12)$ alloys

A. Perumal and V. Srinivas*
Department of Physics, Indian Institute of Technology, Kharagpur-721302, India

K. S. Kim and S. C. Yu
Department of Physics, Chungbuk National University, Cheongju 361-763, Korea

V. V. Rao
Cryogenic Engineering Center, Indian Institute of Technology, Kharagpur-721302, India

R. A. Dunlap
Department of Physics, Dalhousie University, Halifax, Nova Scotia, Canada B3H 3J5

(Received 31 May 2001; revised manuscript received 24 September 2001; published 22 January 2002)

The magnetization as a function of field and temperature has been measured for a series of amorphous $Fe_{90-x}Mn_xZr_{10}$ alloys with $x=0-12$ in the temperature range 4.2–300 K. All the samples of the present study show double transition (reentrant) behavior below room temperature. The high-temperature transition (T_c) decreases linearly at about 6 K/at. % of Mn, while the low-temperature transition (T_{sg}) increases at about 2.6 K/at. % of Mn. A detailed analysis of the temperature dependence of magnetization data reveals: (i) Spin-wave excitations at low-temperature, single-particle excitations and local-spin-density fluctuations (LSDF's) over a wide range of intermediate temperatures and enhanced fluctuations in the local magnetization for temperature close to T_c contribute dominantly to the thermal demagnetization of spontaneous magnetizations; (ii) external applied magnetic field of strength $\geqslant 5$ kOe suppresses the LSDF's; (iii) the spin-wave stiffness constant (D) decreases from 35.6 ± 0.3 to 23.2 ± 0.2 meV Å^2 with increasing Mn concentration; and (iv) the D/T_c ratio remains constant for all the compositions. A study of critical behavior of the magnetic order-disorder transition by various methods suggest that the critical exponents obtained below and above Curie temperature obey a scaling law [$\delta - 1 = \gamma/\beta$ and $\alpha + \gamma = 2(1-\beta)$] with a high degree of accuracy in the asymptotic critical region. The exponents are independent of composition and are in close agreement with the values those predicted for three-dimensional Heisenberg ferromagnets. The magnetic parameters such as high-field susceptibility, coercivity, local magnetic anisotropy, and spin-glass behavior, obtained from the low-temperature magnetization data, are consistent with the presence of a mixed magnetic state. The detailed analysis of high-field thermomagnetization data could be explained in terms of the nearest-neighbor Heisenberg model. Moreover, the temperature dependence of the magnetic behavior is discussed in terms of competing ferromagnetic and antiferromagnetic exchange interactions.

DOI: 10.1103/PhysRevB.65.064428 PACS number(s): 75.50.Kj, 07.55.Jg, 51.60.+a, 75.50.Lk

I. INTRODUCTION

The nature of the transition from a magnetically ordered to disordered state and plausible descriptions of the microscopic states in quenched systems with random exchange interactions have been the topics of recent interest both theoretically and experimentally. The frustration arising as a consequence of exchange interactions of both signs has a variety of manifestations in the observed magnetic properties for glassy ferromagnets; (i) in the ferromagnetic regime, the moments retain some of their randomness even at high fields as large as 200 kOe, (ii) the magnetic isotherms show a large differential susceptibility, and (iii) the spontaneous magnetization that develops in the ferromagnetic state at the Curie temperature (T_c) gets reduced to a small value at a finite temperature well below T_c giving way to a spin-glass-like behavior. Kakehashi[1] has predicted that the local atomic moment on an atom depends on the number of first nearest neighbors. Also the sign of the magnetic coupling changes with the local environments leading to frustration of moments that results in complex magnetic characteristics. One such material that has been thoroughly investigated through various experimental techniques is amorphous (a-)$Fe_{90}Zr_{10}$ alloy. Critical behavior studies,[2–4] which relate various thermodynamical quantities near the ferromagnetic (FM) to paramagnetic (PM) phase transition, have been performed in order to understand the nature of the magnetic phase transition at the Curie point and the type of magnetic ordering below the Curie point. From the detailed and careful analysis of magnetic and transport studies, it has been demonstrated that there is no influence of structural disorder on the values of asymptotic critical exponents that are measured in materials where the critical exponent α for the pure material is negative (i.e., the so-called Harris criterion[5]). On the other hand, the exponents[6] obtained from bulk-magnetization data ($H \leqslant 200$ Oe) in the critical region deviate from the Heisenberg values. Reanalysis of the data indicate the critical exponents[7] obtained in the real critical region are in good agreement with three-dimensional short-range nearest-neighbor Heisenberg ferromagnets (3DHM). The magnetic properties of $Fe_{100-c}Zr_c$ with $c=8$ and 10 showed superparamagnetic behavior above T_c where the mean magnetic moment of the

 ©2002 The American Physical Society

superparamagnetic spin clusters[8] decreased with increasing temperature.[9]

The phenomenon of reentrant spin-glass (SG) behavior usually exhibited by both amorphous and crystalline magnetic systems has also received scientific attention. The nature of the reentrant SG transition has been investigated extensively both theoretically and experimentally. Most of the results were interpreted using the Sherrington and Kirkpatrik[10] model in terms of Ising spins. This theory predicts a double transition PM→FM→SG behavior, but here the lowest temperature SG phase is a pure spin glass and not a mixed FM and SG phase. Later, with isotropic vector spins,[11] it was shown as a mixed phase where a spontaneous magnetization coexists with a SG ordering of the transverse components of the spins. From experimental studies three different views have emerged: (i) a reentrant phase coexisting with the spin clusters of antiferromagnetic Fe spins and a ferromagnetic FeZr matrix in which the spin clusters are frozen in random orientations,[12,13] (ii) the reentrant phase is a mixed phase where the ferromagnetic state co-exists with a transverse SG ordering (XY plane) with spontaneous magnetization in the direction of the broken symmetry[14] (z axis), and (iii) a spin system for temperatures lower than the spin-glass transition temperature that comprises an infinite 3D ferromagnetic network and finite spin clusters (composed of a set of ferromagnetic coupled spins) which are frozen in random directions and embedded in the ferromagnetic matrix.[15] However, the exact nature of the low-temperature transition and that of the reentrant state has eluded clear-cut understanding so far.

The replacement of Fe in Fe rich FeZr alloys by any other transition metal (TM) or metalloid elements brings out drastic changes in their magnetic behavior depending on the nature of the substituting elements.[16–32] When Fe is replaced with Co,[16,25] the T_c increases drastically and the reentrant behavior is completely destroyed, while Cr substitution lowers T_c but low-temperature reentrant SG behavior was not observed.[17] Substitution of Mn decreases the T_c almost linearly and the reentrant behavior is observed up to $x=16$.[33] This enables one to characterize and to understand the development of the reentrant SG behavior over a large concentration range. Recent study of critical behavior of Co substituted amorphous (a-)FeZr alloys demonstrate that the critical exponents[25] and critical amplitudes are consistent with the Harris criterion and the exponents do not depend on the composition. On the other hand, the critical exponents[21] obtained on two of the Mn substituted samples were found to be larger than the values predicted for the 3DHM. Moreover, the exponent values seem to depend on Mn substitution. From a range-of-fit analysis on binary FeZr and ternary Fe-Co-Zr amorphous alloys, Babu *et al.*[22] argued that the anomalously large exponent values observed by Nicolaides *et al.*[21] are average values of the effective critical exponents. As discussed earlier, substitution of Co and Mn in a-$Fe_{90}Zr_{10}$ shows contrasting magnetic behavior making comparison difficult. Subsequently, preliminary analysis on low-temperature ac susceptibility[3] indicated that the amplitudes of the exponents in the real critical region are same as those predicted by 3DHM. Thus no concrete conclusions regarding the nature of the magnetic phase transition at T_c could be drawn from the quantitative comparison between the values of effective critical exponents reported in the literature and those of the asymptotic critical exponents predicted by the theory. Therefore there is an urgent need to carry out a systematic analysis on a series of Mn substituted a-FeZr alloys to investigate the critical behavior as well as the concentration dependence of the exponents. In addition, these alloys are suitable for the study of a reentrant magnetic phase that could be observed over a wide range of concentration.

Systematic magnetization measurements have been performed as a function of temperature in the temperature range 4.2–300 K and field up to 50 kOe for a-$Fe_{90-x}Mn_xZr_{10}$ with $x=0$, 4, 6, 8, 10, and 12 to seek answers to the following questions:

(i) Does the FM order coexists with SG ordering? (or) Is it a pure SG phase due to random freezing of spins at $T<T_{sg}$?

(ii) What is the nature of the magnetization in the so-called FM phase ($T_{sg}\leqslant T\leqslant T_c$) for this kind of alloy system?

(iii) Is the high temperature transition similar to that in conventional ferromagnets? and how do the absence of long-range atomic order and structurally induced exchange fluctuations in these materials influence the critical behavior?

(iv) Do the critical exponents depend on choice of magnetic scaling equation of state?

II. EXPERIMENTAL DETAILS

Amorphous $Fe_{90-x}Mn_xZr_{10}$ ($x=0$, 4, 6, 8, 10, and 12) alloys were prepared by arc melting the high-purity elemental constituents under argon gas atmosphere and by single-roller melt quenching in the form of long ribbons of 1–2 mm width and 20–40 μm thickness. The amorphous nature of the samples was confirmed through x-ray-diffraction studies using $Cu-K_\alpha$ radiation. The composition of the samples were verified through energy dispersive x-ray analysis (EDAX). The analyzed composition is found to be close to the nominal composition at lower Mn concentration and within 0.4% at higher Mn concentration. The magnetization measurements as a function of temperature and field were carried out on a single long ribbon sample using a Quantum Design superconducting quantum interference device (MPMS model) magnetometer with the sensitivity of 10^{-8} emu and a vibration sample magnetometer (Oxford, Maglab model) with the sensitivity of 10^{-7} emu for all samples over the temperature range 4.2–300 K. Since the external applied field was directed along the length of the ribbon and in the plane of the ribbon, demagnetization effects are negligible in the present measurements. The sample temperature was controlled and monitored by using silicon diode sensor and proper care has been taken for in-field magnetic measurements. For critical behavior study, the data were collected in the closed intervals over the temperature range T_c-50 K to T_c+70 K and in magnetic fields up to 60 kOe. Low-field ac susceptibility data[3] have been taken using conventional mutual induction technique to identify the magnetic phase transition temperatures.

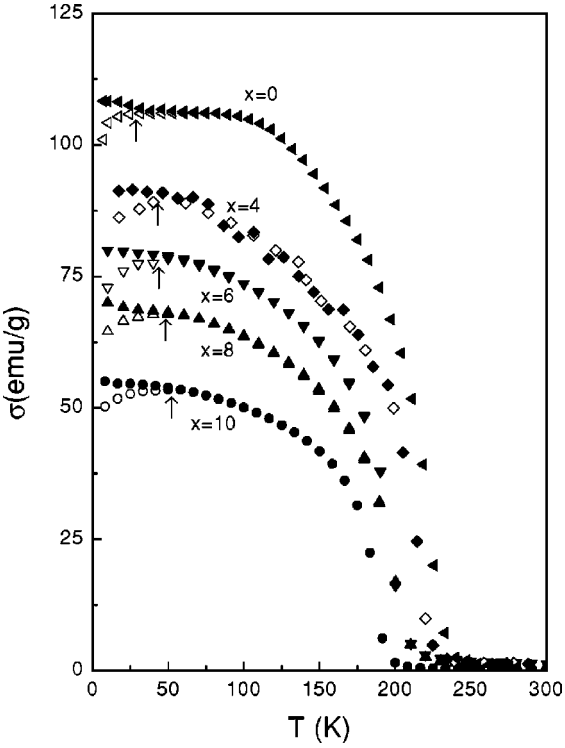

FIG. 1. The field-cooled (solid symbol) and zero-field-cooled (open symbol) magnetization curves in the field of 10 Oe is plotted as a function of temperature for amorphous $Fe_{90-x}Mn_xZr_{10}$ alloys with $x=0$, 4, 6, 8, and 10. Arrow indicates the bifurcation point between the field-cooled and zero-field-cooled data.

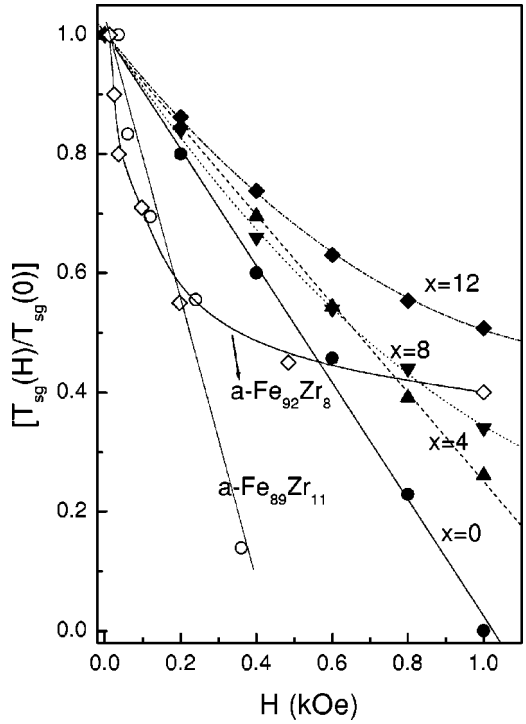

FIG. 2. The normalized value of field dependence of spin-glass transition temperature with respect to zero field is plotted as a function of applied field for amorphous $Fe_{90-x}Mn_xZr_{10}$ alloys. Note: The field dependence of spin-glass transition taken from Ref. 34 for amorphous $Fe_{89}Zr_{11}$ and $Fe_{92}Zr_8$ is also shown in figure for comparison.

III. RESULTS AND DATA ANALYSIS

The zero-field-cooled (ZFC) and field-cooled (FC) magnetization (σ) curves as a function of temperature under the external field of 10 Oe is shown in Fig. 1 for amorphous $Fe_{90-x}Mn_xZr_{10}$ alloys with $x=0$, 4, 6, 8, and 10. The magnetization data measured as a function of temperature show some interesting features: (i) a sharp increase in $\sigma(T)$ at higher temperature (T_c) followed by one more transition at low temperature, i.e., spin-glass-like transition temperature (T_{sg}) where the ZFC and FC curves start to diverge; (ii) all the compositions of the present study show a clear double transition behavior; (iii) the shape of the σ vs T curve is observed to be quite sensitive to the applied magnetic field and σ decreases as Mn concentration increases; and (iv) the transition from PM to FM decreases from 230 to 154 K, while the transition from FM- to SG-like behavior increases from 35 to 65 K as the Mn concentration increases. These observations are in good agreement with our earlier ac susceptibility results.[28] The behavior over specific temperature ranges is described in detail below.

A. $T \leqslant T_{sg}$

The presence of low-temperature transition (T_{sg}) has been confirmed from dc magnetic measurements. FC and ZFC magnetization experiments have been performed with different applied magnetic field up to 1.0 kOe. The zero-field $T_{sg}[T_{sg}(0)]$ is obtained by extrapolating the field dependence of T_{sg} to zero field. As shown in Fig. 2, the low-temperature transition shifts to further lower temperatures with increasing external field, linearly for $x=0$,[15,34] while a nonlinear tendency could be observed for higher Mn concentration alloys. Present results show (i) an increase in T_{sg} with Mn and (ii) the nonlinear tendency in $T_{sg}(H)/T_{sg}(0)$ with applied field indicating an increase in magnetic disorder as the Mn concentration is increased. These observations are similar to FeZr binary alloys[34] and this nonlinear tendency in high Mn concentration samples may be attributed to the magnetic disorder, which could be either due to more frustration or magnetic hardness.[13] The field dependence of T_{sg} shown in Fig. 2, neither follows the A-T (Ref. 35) line nor the G-T line.[11] The observed field dependence is smooth and appears to be saturating at high fields for higher Mn concentration, which is in good agreement with the earlier work on binary FeZr alloys.[14] However, a further work at higher fields is very much essential before drawing a definite conclusion on magnetic structure at lower temperatures.[8] Figure 3 shows a typical field dependence of magnetization curves for $x=0$, 4, 8, 10, and 12 at 4.2 K. The nonsaturation behavior of the magnetization curves in applied fields of more than 60 kOe suggests a possible presence of competing exchange interactions. This argument can be further supported by the decrease of the average magnetic moment (inset of Fig. 3) and T_c (Ref. 28) with increasing Mn concentration. In order to understand the magnetic state at low temperatures, the Arrott plot (AP) is shown in Fig. 4 for $x=0$, 4, 8, 10, and 12

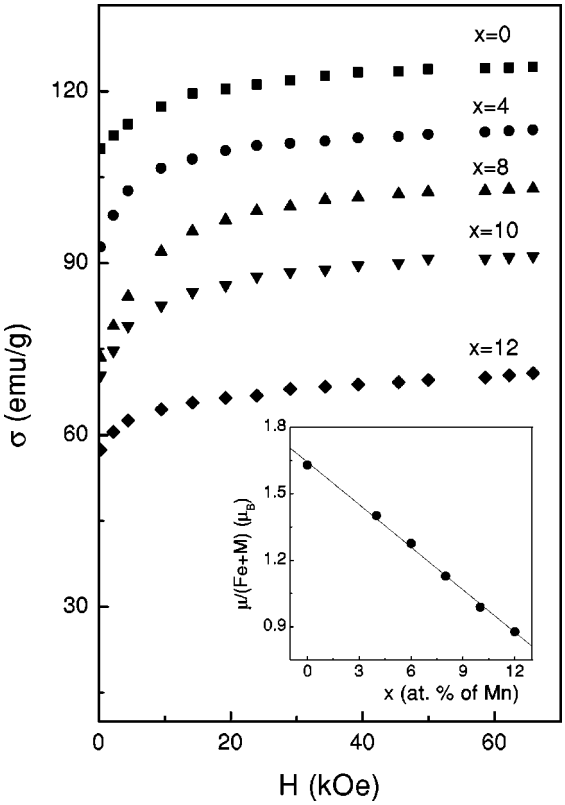

FIG. 3. The magnetic isotherm for amorphous $Fe_{90-x}Mn_xZr_{10}$ alloys with $x=0$, 4, 8, 10, and 12 at 4.2 K. Inset: the average magnetic moment is plotted as a function of Mn concentration.

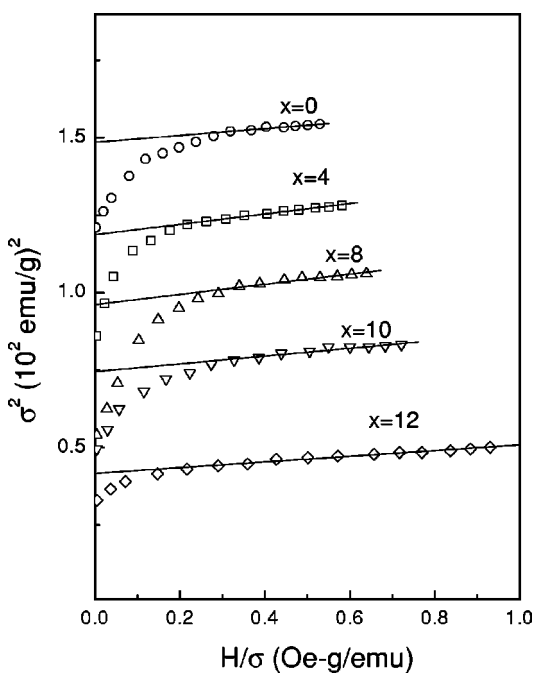

FIG. 4. The Arrott-plot (plot of σ^2 versus H/σ) for amorphous $Fe_{90-x}Mn_xZr_{10}$ alloys with $x=0$ (o), 4 (□), 8 (Δ), 10 (∇), and 12 (◇) at 4.2 K.

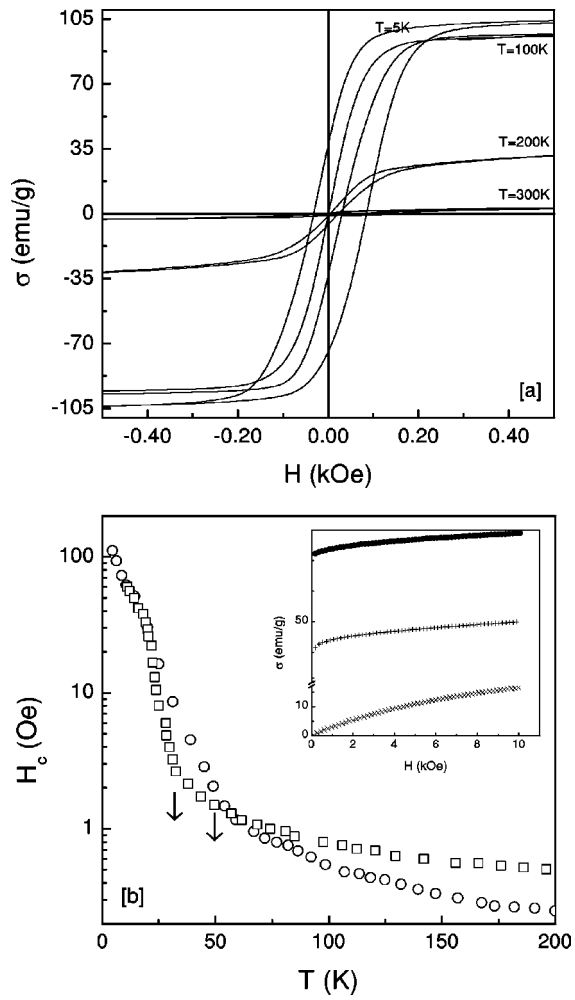

FIG. 5. (a) The hysteresis loop measured at different constant temperatures for amorphous $Fe_{82}Mn_8Zr_{10}$ alloy. (b) The coercivity as a function of temperature for $x=4$(□) and $x=8$ (o). Inset: The isotherm curve at three different temperatures (i) $T\leqslant T_{sg}$(●), (ii) $T_{sg}\leqslant T\leqslant T_c$ (+) and (iii) $T\geqslant T_c$(×)] is plotted for a-$Fe_{86}Mn_4Zr_{10}$ alloy.

at 4.2 K, where the observed behavior implicitly indicates that the magnetic state at low temperature is neither a pure SG state[36] nor a pure FM state. The positive intercept of σ^2 in the AP also indicates the existence of the FM order below T_{sg}. These results suggest a coexistence of FM and SG orders at low temperature due to competing exchange interactions. The development of these interactions can be studied by investigating the field dependence of the magnetization in different temperature regions: (i) $T\leqslant T_{sg}$, (ii) $T_{sg}<T<T_c$, and (iii) $T\geqslant T_c$. The hysteresis loop measurements for amorphous $Fe_{82}Mn_8Zr_{10}$ alloy at different temperature is depicted in Fig. 5(a), while the coercivity obtained from the temperature-dependent hysteresis curves is shown in Fig. 5(b). The field dependence of magnetization curves at different temperature ranges are also shown in the inset of Fig. 5(b) for amorphous $Fe_{86}Mn_4Zr_{10}$ alloys. Although the coercivity starts to develop below T_c, a rapid increase is observed only below T_{sg}. The rapid change in the $H_c$vs T suggests the interrelation between T_{sg} and H_c. The high-field

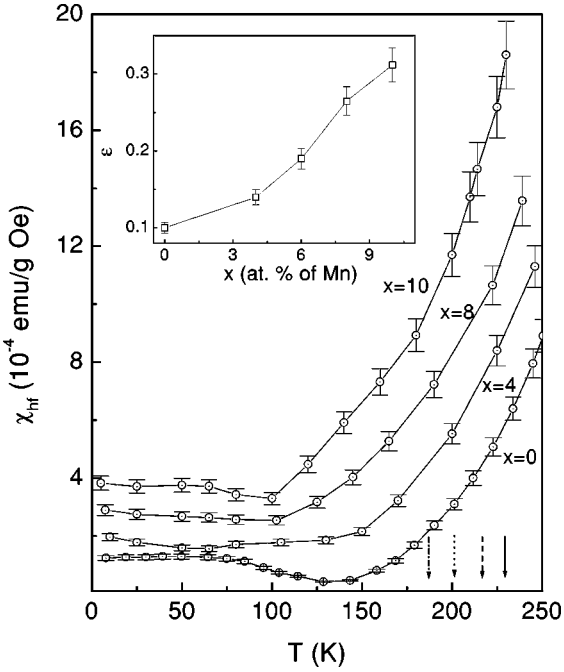

FIG. 6. The high-field susceptibility is plotted against temperature. The arrow indicates the value of T_c for $x=0$ to 10 (from right to left). Inset: the local magnetic anisotropy constant (ϵ) obtained at 4.2 K is plotted as a function of Mn concentration.

slope of the magnetization curves is observed to be large and increases appreciably with Mn concentration.

The high-field region of the σ vs H curve can be best described by an analytical expression, $\sigma(H)=\chi_{hf}H+\sigma_0(1-\epsilon H^{-\phi})$, where χ_{hf} is the high-field susceptibility, σ_0, ϵ (the local magnetic anisotropy), and $\phi(=0.5)$ are constants. In order to determine the various physical parameters with more accuracy, a detailed nonlinear fitting procedure is carried out as follows: Initially, the second term in an analytical expression is set equal to zero and a detailed range-of-fit analysis is carried out on magnetization data that includes the first term only. In this case, χ_{hf} is treated as free parameter and the minimum field range (H_{min}) is fixed at the value for the data point close to 1 kOe, while the upper value H_{max} is varied. It is observed from the analysis that over a certain range near high field, the value of the free parameter is unaffected within the experimental error. The coefficient of the first term is defined at the value calculated from the previous analysis and the range-of-fit analysis is performed in the high-field region with both terms included and all other parameters treated as free. The increase of local magnetic anisotropy (inset of Fig. 6) with Mn concentration and the high-field susceptibility as a function of temperature for $x=0$, 4, 8, and 10 are shown in Fig. 6. The value of χ_{hf} increases with increasing Mn concentration and it decreases rapidly as the temperature is lowered below T_c and goes through a broad minimum before attaining a constant value at lower temperature. This is a typical character of the itinerant ferromagnets. In the case of conventional ferromagnets, the high-field susceptibility decreases from the Curie point continuously and it approaches zero at 0 K. The large value of χ_{hf} along with low values of magnetic moment and T_c are the indicative of typical itinerant character.

B. $T_{sg} \leqslant T \leqslant T_c$

It is well known that in most of the Fe based amorphous and crystalline alloys the spin-wave (SW) excitations are found to dominate the magnetic behavior over a wide temperature range.[26,37] However, in some cases the presence of additional Stoner single-particle (SP) excitations were confirmed through the detailed analysis of inelastic neutron-scattering measurements.[38,39] To identify the individual contribution of SW and SP excitations, the magnetization data as a function of temperature were taken at constant field of 10 kOe in the temperature range of 4.2–300 K at 0.3-K intervals for $x=0$–12. The relative deviation of in-field magnetization from its value at 0 K [the value at 4.2 K is extended to 0 K and the value at 0 K is taken as $\sigma(H,0)$], i.e., $\{[\sigma(H,0)-\sigma(H,T)]/\sigma(\mathrm{H},0)\}=\Delta\sigma(T)$ is plotted against the reduced temperature T/T_c. In order to examine the contribution of various excitations, the magnetization data have been analyzed in the light of both SW theory as well as Stoner excitations.[40–42] The weak itinerant character can be verified through these studies in the FM region. The excitations from the SW and SP are nearly independent of each other and the thermal demagnetization due to SW and SP is given by the sum of the both contributions,

$$\Delta\sigma(T)=\Delta\sigma_{SW}(T)+\Delta\sigma_{SP}(T), \tag{1}$$

where the $\sigma_{SW}(T)$ and $\sigma_{SP}(T)$ contributions to $\Delta\sigma(T)$ are given by

$$\Delta\sigma_{SW}(T)=AT^{3/2}(1-D_1T^2-D_2T^{5/2})^{-3/2}\times\mathcal{Z}\left(\frac{3}{2},\frac{T_g}{T}\right)+BT^{5/2}\mathcal{Z}\left(\frac{5}{2}\frac{T_g}{T}\right) \tag{2}$$

and

$$\Delta\sigma_{SP}(T)=XT^{3/2}e^{(-\Delta/k_BT)} \tag{3}$$

for strong itinerant ferromagnet,[40–42]

$$\Delta\sigma_{SP}(T)=YT^2 \tag{4}$$

for weak itinerant ferromagnet.[40–42]

According to spin-wave theory, the relation between the coefficients $A(B)$ of the $T^{3/2}(T^{5/2})$ terms in Eq. (2), the spin-wave stiffness constant and the average mean-square range of exchange interactions, can be written as

$$D(0)=\frac{k_B}{4\pi}\left(\frac{\zeta(3/2)g\mu_B}{\sigma(0)A\rho}\right)^{2/3}, \tag{5}$$

$$\langle r^2\rangle=\zeta^{-1}\left(\frac{5}{2}\right)\left(\frac{4B\sigma(0)}{3\pi g\mu_B}\right)\left(\frac{4\pi D}{k_B}\right)^{5/2}, \tag{6}$$

where $\zeta(3/2)=2.612$ and $\zeta(5/2)=1.342$ are the Riemann ζ function and ρ is the density. Since $t_H=(T_g/T)$ is less than 1 ($t_H \ll 1$) in the present temperature range, the functions $\mathcal{Z}(3/2,T_g/T)$ and $\mathcal{Z}(5/2,T_g/T)$ were defined in the earlier

analysis.[41] A nonlinear least-square-fit program is used to analyze the magnetization data for alloys with $x=0-12$ using Eq. (2) including all the parameters. In order to highlight the dominant contribution, initially, the reduced magnetization is plotted against different functional dependences of temperature, which helps to confirm the dominant contribution individually at different temperature ranges. The fitting procedure[43] is carried out considering only the SW excitation contribution in the low-temperature range from 5 to 40 K. Realizing the fact that besides the contribution of SW there exist SP excitations, which also contribute to the low-temperature magnetization of the ferromagnet, the next step of the data analysis is to include in Eq. (2) an additional term, either Eq. (3) or Eq. (4), which denotes the SP excitation. The fitting procedure is carried out with all possible combinations based on Eq. (2)–(4), i.e., the cases (i) $B=X=Y=0$, (ii) $B\neq 0$, $X=Y=0$, (iii) $B=X\neq 0$, $Y=0$, (iv) $B=X=0$, $Y\neq 0$, (v) $B=0$, $X=Y\neq 0$, (vi) $B=Y=0$, $X\neq 0$, (vii) $\sigma_{SW}(T)$: $A=0$; $B\neq 0$, (viii) $\sigma_{SW}(T)$: $A\neq 0$; $B=0$, (ix) Eq. (3) alone, and (x) Eq. (4) alone, corresponding to the fits based on (i) $T^{3/2}$ term alone [one free parameter (FP)], (ii) $T^{3/2}+T^{5/2}$ terms (two FP's), (iii) $T^{3/2}+T^{5/2}+T^{3/2}e^{(-\Delta/k_BT)}$ terms (four FP's), (iv) $T^{3/2}+T^2$ terms (two FP's), (v) $T^{3/2}+T^2+T^{3/2}e^{(-\Delta/k_BT)}$ terms (four FP's), (vi) $T^{3/2}+T^{3/2}e^{(-\Delta/k_BT)}$ terms (three FP's), (vii) $T^{5/2}$ term alone (one FP), (viii) $T^{3/2}$ term alone (one FP), (ix) $T^{3/2}e^{(-\Delta/k_BT)}$ term alone (two FP's), and (x) T^2 term alone (one FP), respectively. In the range-of-fit analysis, the values of the free parameters and quality of fits are continuously monitored for all possible cases as the temperature interval $T_{min}\leqslant T\leqslant T_{max}$ is progressively narrowed down either by keeping T_{min} fixed at a given value and lowering T_{max} in steps of 2–3 K towards T_{min} or by keeping T_{max} fixed at a certain value and raising T_{min} towards T_{max}. The minimum in χ^2, which gives the best description of data, is defined as

$$\chi_r^2=\left(\frac{1}{N_p-N_T}\right)\sum_1^N\left(\frac{(\Delta\sigma_{theo.}-\Delta\sigma_{exp.})^2}{\sigma^2}\right), \qquad (7)$$

where N_p is the total number of data points that are covered within the temperature range for fitting procedure and N_T is number of free parameters used for the analysis. Such a choice enables one to make an unambiguous assessment of the quality of not only a given type of fit as a function of T_{min} and T_{max}, but also of different types of fits in the same temperature interval.

The fit to Eq. (2) considering only SW contribution without the $BT^{5/2}$ and YT^2 terms yields $\chi^2=2\times 10^{-5}$, which is almost one order of magnitude less than the minimum possible experimental errors. However, the data when fitted to Eq. (1), i.e., a combination of Eqs. (2) and (4), along with $BT^{5/2}$ term (five FP's including D_1 and D_2) yields an improved $\chi^2=1\times 10^{-10}$, while the expression given by Eq. (3) does not describe the magnetization data over any temperature interval and the fit yields unphysical values for the parameters X and Δ. The observed values of D_1 and D_2 are very small compared to the other systems.[48] So, the fitting procedure is carried out by neglecting the contribution from D_1 and D_2 terms in Eq. (2) and the final form of the equation is defined as

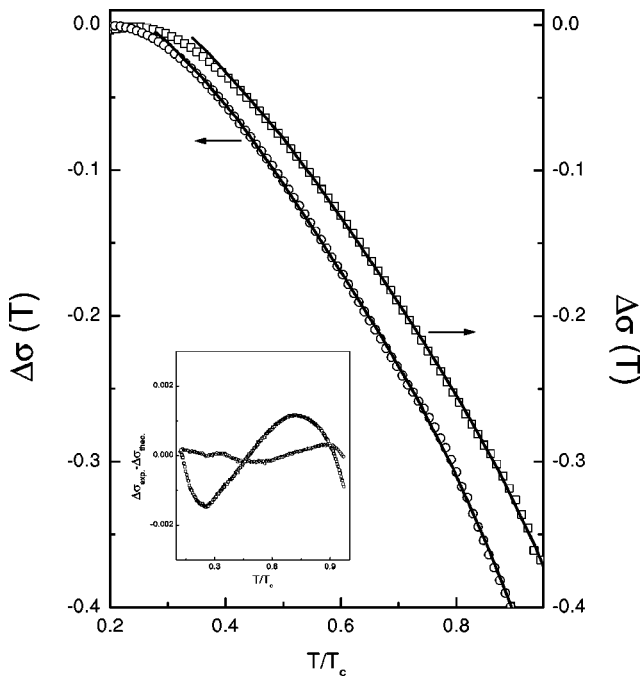

FIG. 7. The reduced magnetization is plotted against reduced temperature for a-$Fe_{90-x}Mn_xZr_{10}$ alloys with $x=4$ (o) and 8 (□). Note that only one-seventh of the actual data are shown for the sake of clarity. The solid curves through the data points are the theoretical variations predicted by Eq. (1), which combines Eqs. (2) and (4) with the choice of parameters listed in Table I. Inset: the difference between experimental and theoretical data [(□) Eq. (2) + Eq. (3), (o) Eq. (2) + Eq. (4)] is plotted as a function of reduced temperature.

$$\Delta\sigma(T)=AT^{3/2}\mathcal{Z}\left(\frac{3}{2},\frac{T_g}{T}\right)+BT^{5/2}\mathcal{Z}\left(\frac{5}{2}\frac{T_g}{T}\right)+YT^2. \qquad (8)$$

As shown in Fig. 7, the experimental data and best-fitted curves are almost indistinguishable. The determined values of the parameters D, Y, and B are shown in Figs. 8(a) and (b), respectively, as a function of Mn concentration and some other important parameters are listed in Table I. This indicates that a combination of both SW and Stoner SP excitations describes the thermomagnetization curve quite well. The value of spin-wave coefficient (A) is almost two orders[15] of magnitude greater than for pure Fe and Ni ($\simeq 10^{-6}\,K^{-3/2}$).

C. $0.9T_c\leqslant T\leqslant 1.2T_c$

The conflicting[6,12,21,25] results for the critical behavior of the magnetic order-disorder phase transition reported in the literature for weak itinerant amorphous alloys prompted us to carry out a detailed study of the critical behavior near the magnetic phase transition by determining the critical exponents and the Curie temperature from the zero-field quantities such as the inverse zero-field susceptibility (χ_0^{-1}) and

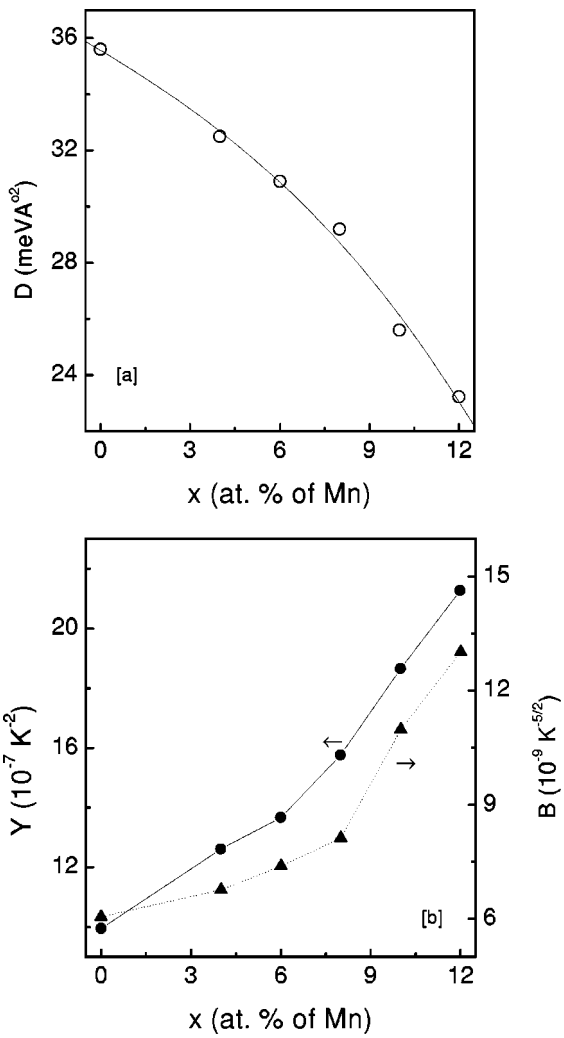

FIG. 8. The various parameters such as (a) spin-wave stiffness constant (D) (b) Y and B, obtained from fitting of magnetization data using Eq. (1) are plotted as a function of Mn concentration for a-$Fe_{90-x}Mn_xZr_{10}$ alloys.

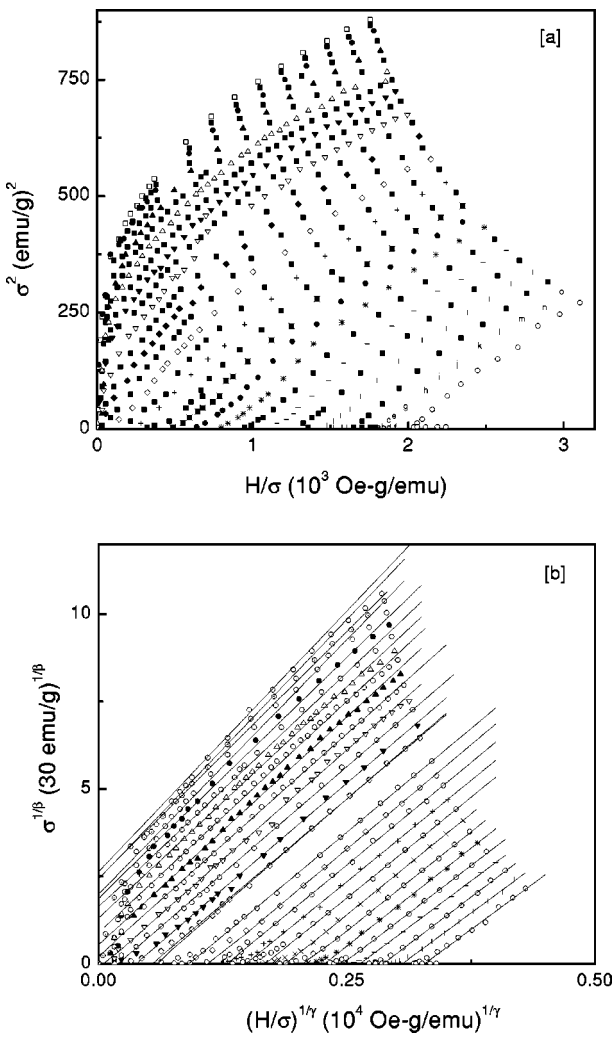

FIG. 9. (a) The Arrott plot, σ^2 versus (H/σ), (b) isotherm curves of $\sigma^{1/\beta}$ versus $(H/\sigma)^{1/\gamma}$, in the temperature range near the critical region for a-$Fe_{82}Mn_8Zr_{10}$ alloy.

the spontaneous magnetization (σ_s), obtained from magnetic isotherm curves in the immediate vicinity of Curie point. The magnetic order-disorder phase transition is characterized by a set of critical exponents γ, β, and δ and these critical exponents are interrelated by the Rushbrook's and Widom scaling relations, defined as $\delta=1+\gamma/\beta$ and $\alpha+2\beta+\gamma-2=0$.

Figure 9(a) shows the AP for a-$Fe_{82}Mn_8Zr_{10}$, where the isotherm shows a set of curved (positive) features just below

TABLE I. The theoretical fit of parameters to Eq. (1) (see text) that combines Eqs. (2) and (4) in the low-temperature range, intermediate temperature range, and temperature close to T_c. Numbers in parentheses denote the estimated uncertainty in the least significant figure.

x	T_c (K) [a]	T_c (K) [b]	T_{sg} (K) [a]	T_{sg} (K) [b]	A ($10^{-4}K^{-3/2}$)	$D(0)$ meV Å^2	$\langle r^2\rangle$ Å^2	χ_r^2 (10^{-10})
0	227 (2)	226 (2)	36 (2)	35 (3)	2.924 (12)	35.6 (9)	5.20 (15)	2.89
4	214 (1)	213 (2)	46 (1)	46 (2)	3.194 (17)	32.5 (6)	3.53 (19)	1.05
6	196 (2)	197 (3)	50 (2)	49 (3)	3.644 (9)	30.9 (7)	3.12 (11)	1.59
8	187 (3)	185 (2)	54 (2)	55 (3)	3.190 (11)	29.2 (4)	2.75 (9)	2.25
10	169 (2)	170 (3)	59 (2)	60 (2)	4.552 (8)	25.6 (5)	2.48 (12)	1.86
12	154 (1)	156 (2)	65 (2)	67 (3)	5.232 (7)	23.2 (10)	1.97 (10)	1.99

[a]The value of T_c and T_{sg} obtained from the magnetization study.
[b]The value of T_c and T_{sg} obtained from the ac susceptibility study (Ref 33).

TABLE II. The value of the Curie temperature obtained from magnetization measurement, critical exponents used for constructing the Modified-Arrott plot (MAP) and the Curie temperature, critical exponents obtained from the Simple power-law (SPL) method. Numbers in parentheses denote the estimated uncertainty in the least significant figure.

x	T_c (K)	MAP plot β	MAP plot γ	SPL method T_c^- (K)	β_{eff}	σ_0^{eff} (G)	T_c^+ (K)	γ_{eff}	σ_0/h_0 (10^{-3})
0	227	0.345 (6)	1.395 (10)	226.9	0.37 (3)	850 (15)	227.5	1.38 (5)	2.56 (8)
4	213	0.369 (9)	1.368 (9)	214.6	0.39 (4)	823 (11)	213.4	1.37 (8)	2.73 (10)
6	197	0.341 (3)	1.358 (6)	198.6	0.33 (2)	810 (9)	195.6	1.35 (5)	2.95 (7)
8	185	0.365 (5)	1.387 (12)	186.3	0.37 (4)	790 (11)	185.3	1.36 (2)	3.23 (5)
10	169	0.368 (6)	1.384 (8)	170.2	0.41 (2)	771 (12)	168.5	1.34 (9)	3.98 (12)
12	154	0.359 (9)	1.378 (5)	154.6	0.39 (5)	755 (9)	154.2	1.39 (5)	4.56 (9)

and above T_c. The usual procedure for extracting σ_s from σ vs H isotherms is to make use of the well-known AP. According to mean-field theory, the σ^2vs H/σ isotherms should give a set of straight lines [known as Arrott-Kouvel (AK) plots] just below and above T_c. The absence of linear behavior in Fig. 9(a) suggests that the mean-field theory is not valid for our present case. Often a modified Arrott plot (MAP) or the Arrott-Noakes[44] plot is used to obtain a straight-line fit,[25,30,45]

$$\left(\frac{H}{\sigma}\right)^{1/\gamma}=\frac{T-T_c}{T_x}+\left(\frac{\sigma}{\sigma_x}\right)^{1/\beta}, \tag{9}$$

where T_x and σ_x are constants that depend on the material. In order to construct the MAP, a prior knowledge of the values of the critical exponents or at least an intelligent guess of the values of γ and β for the system is necessary. Using reasonable values, MAP plots are constructed from which σ_s and χ_0^{-1} values are obtained at various temperatures. From σ_s and χ_0^{-1}, the straightforward method of finding the critical exponents is to use double logarithmic plots of the related quantities. However, all the above methods give best results only when one draws the MAP from proper starting values of γ and β. Therefore, to avoid uncertainties in guessing the values of γ and β, we have followed different independent procedures to analyze the data. The values of γ and β are treated as free parameters and the $\sigma^{1/\beta}$ vs $(H/\sigma)^{1/\gamma}$ isotherms are fitted to straight lines. The average χ^2_{fit} is a minimum for which the linear isotherm at T_c, when extrapolated, passes through the origin. This procedure gives the best values of γ and β (listed in Table II) for which all the isotherms are linear in the immediate vicinity of T_c. The above procedure is repeated for various starting values of γ and β until stationary values of γ and β are obtained. A typical MAP diagram constructed with the exponents obtained from the fitting of a-$Fe_{82}Mn_8Zr_{10}$ magnetization data in the actual critical region is shown in Fig. 9(b), where only one-half of the actual data are shown for the sake of clarity. All the samples of present investigation show similar plots in the actual critical region. This method permits the accurate determination of the zero-field quantities through proper choice of critical exponents γ and β from the intercepts $[\sigma(0,\mathrm{T})]^{1/\beta}$ and $[\chi_0^{-1}(0,\mathrm{T})]^{1/\gamma}$ that MAP isotherms make with the ordinate for $T\leqslant T_c$ and with the abscissa for $T\geqslant T_c$, respectively, when their high-field regions are extrapolated to $(H/\sigma)^{1/\gamma}=0$ and $\sigma^{1/\beta}=0$. The values of σ_s and χ_0^{-1} as computed from these intercepts are plotted against the temperature in Fig. 10 for $x=4$, 8, and 12. The data are fitted using the single power-law (SPL) and Kouvel-Fisher (KF) methods, which are described as follows:

$$\left.\begin{aligned}\sigma_s(\eta)&=\sigma_0^{eff}(-\eta)^{\beta_{eff}}, &\eta<0\\ \chi_0^{-1}(\eta)&=\left(\frac{h_0}{\sigma_0}\right)^{eff}\eta^{\gamma_{eff}}, &\eta>0\end{aligned}\right\}. \tag{10}$$

A detailed analysis of the data based on the above equation shows that the critical exponents depend on the temperature range selected for fitting procedure. So, this method of analysis provides only the effective exponents (Table II). The effective exponent of the present analysis as a function of the temperature range chosen for fitting is shown in Fig. 11.

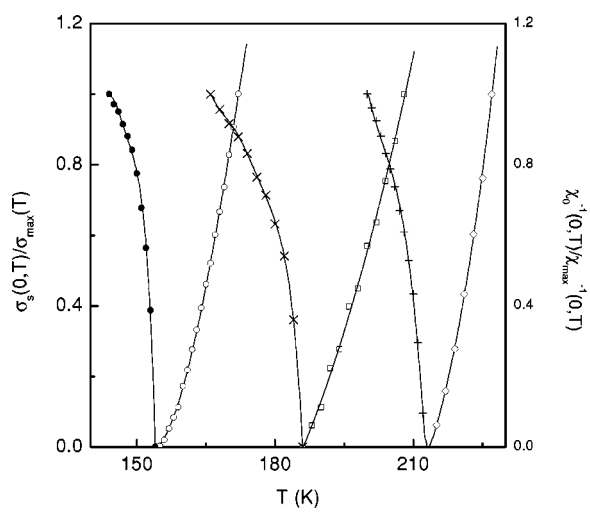

FIG. 10. Normalized values of temperature variation of spontaneous magnetization (left-hand axes), and zero-field susceptibility (right-hand axes), along with the fit obtained with the help of a simple power law for a-$Fe_{90-x}Mn_xZr_{10}$ alloys with $x=4(+,\diamond)$, $8(\times,\square)$, and 12 (●, o).

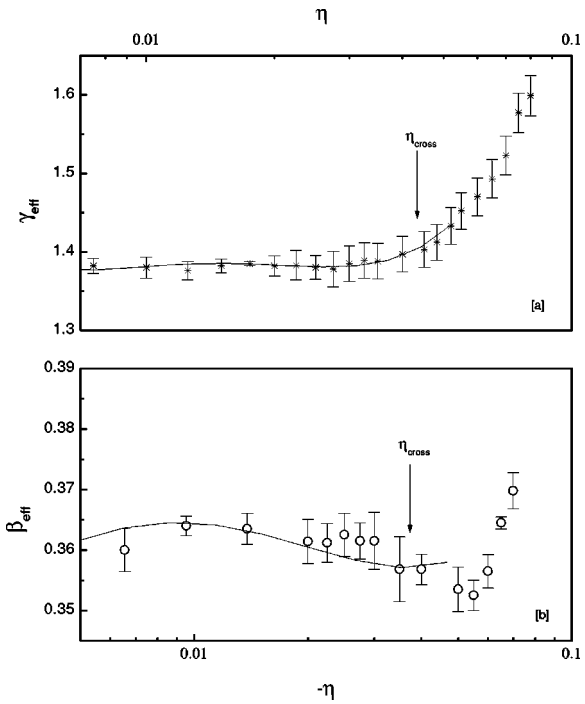

FIG. 11. The effective values of exponents (a) γ and (b) β plotted against reduced temperature, $\eta=(T-T_c)/T_c$, for a-$Fe_{78}Mn_{12}Zr_{10}$ alloy.

In order to determine the critical exponents and the Curie temperature with high precision, the Kouvel-Fisher method[46] is followed. This method is an alternative analytical expression of SPL, defined as

$$\left.\begin{aligned} C_{KF}(T)&=\left(\frac{d(ln(\chi_0^{-1}))}{dT}\right)^{-1}=\left(\frac{\eta T_c}{\gamma}\right)\\ D_{KF}(T)&=\left(\frac{d(ln(\sigma_s))}{dT}\right)^{-1}=\left(\frac{\eta T_c}{\beta}\right)\end{aligned}\right\}, \tag{11}$$

where $\eta=[T-T_c]/T_c$. According to this method, the quantities $C_{KF}(T)$ and $D_{KF}(T)$ plotted against a reduced temperature range give a straight line with the slopes $(1/\gamma)$ and $(1/\beta)$, respectively, with an intercept on the η axis, which is equal to T_c. Figure 12 shows the plot of $C_{KF}(T)$ and $D_{KF}(T)$ as a function of reduced temperature range for amorphous $Fe_{90-x}Mn_xZr_{10}$ alloys with $x=4$, 8, and 12. The solid line passing through the data points is the best fit to the data using Eq. (11) and the obtained value of critical exponents and Curie temperature are listed in Table III. One advantage of this method is that one does not need to know the value of T_c and also it provides a consistency condition for T_c, namely, both $C_{KF}(T)$ vs T and $D_{KF}(T)$ vs T should provide the same value of T_c.

Scaling analysis helps to check the validity of the magnetic scaling equation of state (MSES) and makes use of a specific form of scaling equation of state to simultaneously determine the exponents β and γ or β and δ from the in-field magnetization data. Two different methods of analysis are performed on $\sigma(H,T)$ data, in order to determine whether or not the values of critical exponents depend on the

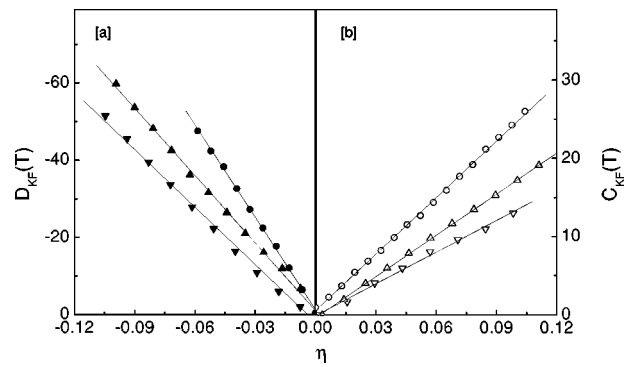

FIG. 12. (a) $D_{KF}(T)$ against η and (b) $C_{KF}(T)$ against η, in the critical region for amorphous $Fe_{90-x}Mn_xZr_{10}$ alloys with $x=4$, 8, and 12. The lines passing through the data points show the best fit to Eq. (11).

selection of magnetic scaling equation of state for analysis. In this method, the scaling equation of state is in the form of

$$\left(\frac{H}{|\eta|^{\beta+\gamma}}\right)=f_{\pm}\left(\frac{\sigma}{|\eta|^{\beta}}\right), \tag{12}$$

where the $\pm$ sign refers to the sign of η, $\sigma_m[=\sigma/|\eta|^{\beta}]$ and $h[=H/|\eta|^{\beta+\gamma}]$ are the scaled magnetization and scaled field with respect to the critical exponents, respectively. According to Eq. (12), the σ vs H isotherms in the critical region fall into two universal curves (f_+ for $\eta>0$ and f_- for $\eta<0$) through a proper choice of parameters T_c, β, and γ. The applicability of the above procedure is depicted in Fig. 13 for $x=6$. It is clearly observed from this analysis that the critical exponent values obtained in this way are only the effective values, which depend on the temperature range. These results are summarized in Table IV. An alternative form of the scaling equation of the state is

$$\sigma_m^2=\mp u_{\mp}+v_{\mp}\left(\frac{h}{\sigma_m}\right), \tag{13}$$

where $u_{\mp}$ and $v_{\mp}$ are related to critical amplitudes to determine the critical exponents β and γ. As shown in the inset of Fig. 13 for the temperature in the vicinity of T_c, the plots corresponding to $\sigma_m^2[\sigma^2/|\eta|^{2\beta}]$ vs h/σ_m indeed lie in two

TABLE III. The value of Curie temperature, critical exponents obtained from the Kouvel-Fisher (KF) method over a limited temperature range below and above the magnetic phase transition temperature. Numbers in parentheses denote the estimated uncertainty in the least significant figure.

x	Range of fit	KF method			
	$\eta(10^3)$	β	γ	T_c^-	T_c^+
0	0.9-39	0.353 (9)	1.386 (3)	226.8 (4)	227.0 (2)
4	1-40	0.365 (6)	1.375 (5)	213.2 (6)	213.4 (1)
6	0.5-50	0.351 (4)	1.351 (7)	196.8 (4)	197.0 (3)
8	0.1-30	0.375 (5)	1.368 (8)	185.1 (5)	185.3 (3)
10	1-25	0.346 (3)	1.349 (5)	169.2 (8)	168.9 (5)
12	2-32	0.369 (3)	1.396 (7)	153.9 (3)	154.2 (2)

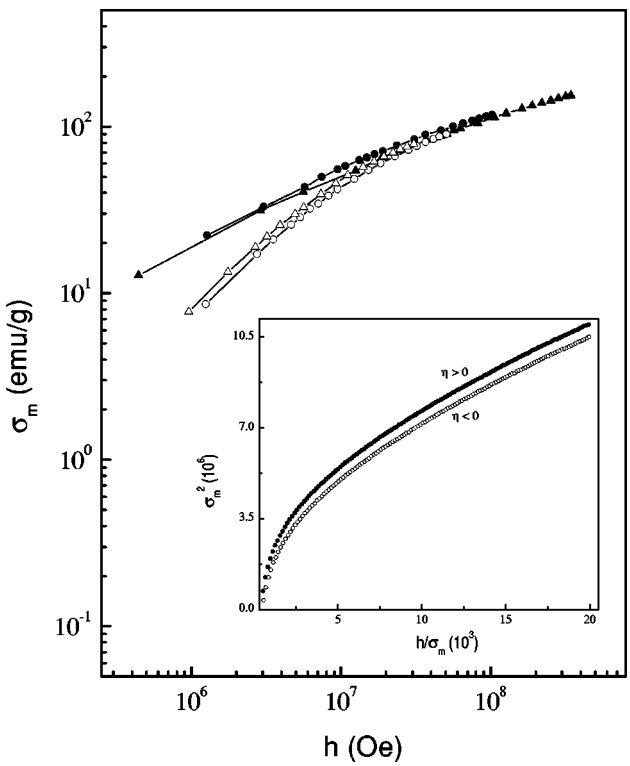

FIG. 13. The scaling plot on log-log scale based on Eq. (11) of the magnetic scaling equation of state for a-$Fe_{84}Mn_6Zr_{10}$ alloy. Inset: σ_m^2 versus h/σ_m scaling plots based on Eq. (12) of magnetic scaling equation of state for a-$Fe_{86}Mn_4Zr_{10}$ alloy.

universal curves, one for $T>T_c$ and the other for $T<T_c$, through a proper selection of parameters T_c, γ, and β. This particular method of analysis provides more accurate values of γ, β, and T_c compared to the earlier analysis [Eq. (12)], since slight deviations of the data from the universal curves are not readily visible in the double logarithmic plot but these become more perceivable in σ_m^2 vs h/σ_m plots. The resulting parameter values are listed in Table IV. The values of the critical exponents obtained from this analysis are close to the asymptotic ones when the value of $\eta \rightarrow 0$.

The critical exponent δ can be determined by analyzing σ-H isotherms near T_c. The log plot of σ-H at $T=T_c$ should yield a straight line with slope $1/\delta$ and an intercept on the ordinate equal to critical amplitude. Figure 14 shows the log-log plot constructed using σ-H isotherms in the vicinity of T_c for the $x=12$ sample. This clearly demonstrates that the isotherm is indeed a straight line at $T=T_c$ and isotherms on either side of T_c exhibit a convex upward and concave downward for temperature $T<T_c$ and $T>T_c$, respectively. The values of the exponent determined from the double logarithmic plot and extracted from the Rushbrook's relation (see Table IV) are in good agreement.

IV. DISCUSSION

The determination of the critical exponents based on asymptotic analysis mainly depends on the choice of the temperature range included in the fitting procedure and results denote the average values over this temperature range.[45]

TABLE IV. The value of critical exponents obtained from the magnetic scaling equation of state and critical isotherm analysis of the magnetization data. Numbers in parentheses denote the estimated uncertainty in the least significant figure.

x	Method	T_c (K)	β_{eff}	γ_{eff}	δ	δ_{RR}[a]
	MSES I	228.3	0.371 (21)	1.392 (17)		
0	MSES II	226.8	0.365 (18)	1.365 (15)		
	isotherm	227.1			4.75 (7)	4.74
	MSES I	214.5	0.386 (23)	1.367 (13)		
4	MSES II	213.4	0.371 (15)	1.386 (9)		
	isotherm	213.8			4.76 (4)	4.735
	MSES I	195.4	0.372 (16)	1.356 (16)		
6	MSES II	196.9	0.362 (24)	1.379 (19)		
	isotherm	197.1			4.78 (4)	4.801
	MSES I	183.5	0.346 (30)	1.365 (19)		
8	MSES II	185.3	0.365 (23)	1.383 (21)		
	isotherm	185.1			4.79 (3)	4.785
	MSES I	168.2	0.356 (11)	1.346 (16)		
10	MSES II	169.1	0.362 (19)	1.379 (8)		
	isotherm	169.0			4.83 (3)	4.872
	MSES I	153.2	0.382 (13)	1.401 (10)		
12	MSES II	154.1	0.358 (9)	1.368 (8)		
	isotherm	153.9			4.81 (2)	4.823

[a] δ_{RR}: The critical exponent is determined from the Rushbrook's relation $\delta=1+\gamma/\beta$.

The critical exponents obtained from the SPL and KF methods are consistent with each other. In order to demonstrate the way in which the effective values of the exponents depend on the temperature range we followed the expression[3] that can be obtained from the KF relation defined as

$$\beta^*(T)=\left(\frac{\eta T_c}{D_{KF}(T)}\right), \tag{14}$$

$$\gamma^*(T)=\left(\frac{\eta T_c}{C_{KF}(T)}\right). \tag{15}$$

The value of β^* and γ^* obtained for different temperature ranges within the asymptotic critical region are plotted as a function of reduced temperature on a logarithmic scale in Fig. 11. The value of critical exponents for a-$Fe_{90-x}Mn_xZr_{10}$ alloys are close to those predicted for the 3D Heisenberg ferromagnet. The results of the present investigation make it clear that unphysically large exponent values as well as the spread in the exponent values reported in earlier studies are results from the analysis carried out on the bulk magnetization data taken outside the critical region. This is clear as even in the real critical region the exponents depend on tem-

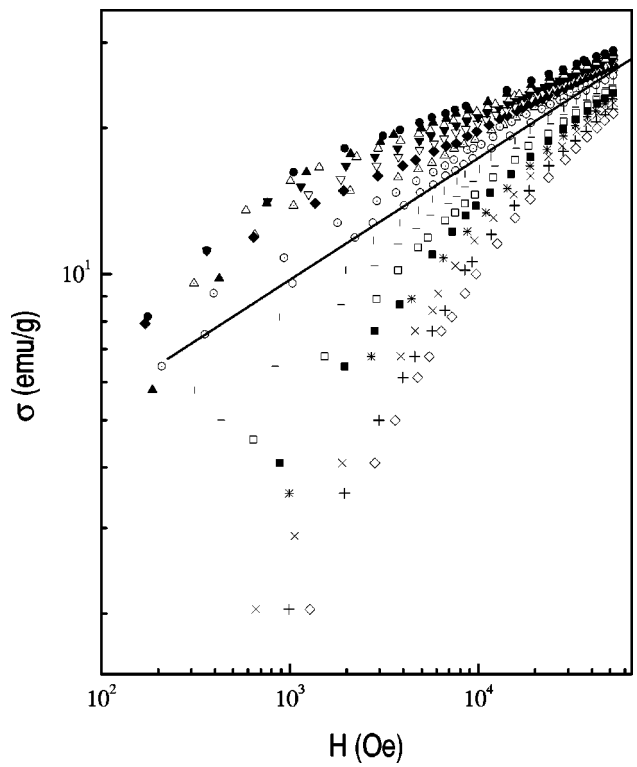

FIG. 14. σ vs H isotherms in a log scale at few selected temperatures just below, above, and at T_c for a-$Fe_{78}Mn_{12}Zr_{10}$ alloy.

perature range and possess much larger values for $\eta > \eta_{cross}$. The main observations that are observed from our analysis are:

(i) The values of critical exponents are independent of Mn substitution within the experimental error in the actual critical region.

(ii) The scaling relation is satisfied to a far greater accuracy by the asymptotic critical exponents than by effective ones.

(iii) The agreement between experimental and theory is better for asymptotic exponents than for their effective counterparts.

The present systematic analysis of magnetization data using various methods on a series of amorphous reentrant SG alloys clearly demonstrates that the larger values of exponents reported by Nicolaides *et al.*[21] are not the asymptotic values but the average effective exponent values that are obtained from the data taken either partially or completely outside the critical region. The present values of the critical exponents are very close to the values that are predicted for the 3D Heisenberg ferromagnet. This suggests that the presence of disorder and composition has no influence on critical behavior of the amorphous systems.[25,47] Moreover, this behavior is also supported by detailed low-field ac susceptibility measurements.[29]

The obtained results of the critical behavior in the present investigation find an explanation in terms of the infinite FM matrix plus finite FM spin clusters model, proposed by Kaul.[15] According to this model, in the temperature range well below $T_c(T<T_c)$, the FM coupling between the spins that makes up the spin clusters is stronger than that between the spins of the FM matrix. As the temperature increases towards T_c, the exchange interaction between the spins in the FM matrix weakens, while the FM coupling between the spins within the spin clusters are relatively strong. Subsequently, the number of spins in the FM matrix decreases rapidly as $T \rightarrow T_c$, so that only a small fraction of spins that participate in the FM-PM phase transition at T_c. The effect of Mn substitution in Fe-Zr is to (i) increase the size as well as number of finite spin clusters, (ii) decrease the number of spins in the FM matrix. This implies that the Mn substitution reduces the number of spins available on the FM matrix, in other words, the fraction of spins participating in the FM-PM transition at T_c decreases with increasing Mn substitution. Since the spin-spin correlation length $\xi(T)$ diverges at T_c,[3] the presence of finite spin clusters is not at all felt for the temperature close to T_c in lower Mn concentration. From this, it is clear that the amorphous and crystalline ferromagnets exhibit a similar behavior in the real critical region and both are showing completely different behavior as the region comes out of real critical region.[49] As the temperature increased beyond T_c, the magnetic inhomogeneity in the spin system is no longer averaged out and γ_{eff} begins to increase and attains a peak value. In this context, it should be noted that so long as the spin-spin correlation length greatly exceeds the size of the largest spin clusters in the spin system, no distinction is made between a homogeneous and inhomogeneous magnetic system for temperatures in the immediate vicinity of T_c.

The parameter values obtained from the magnetization data analysis using SW and SP excitations are shown in Figs. 8 and 15 along with the values of D obtained for different systems for comparison.[48] The value of D decreases with Mn concentration (Fig. 8), while the ratio between D and T_c remains constant [inset (a) of Fig. 15] for all the compositions of the present investigations. Moreover, Fig. 15(b) demonstrates that $1/A \propto T_c^{3/2}$ indicating the validity of Eq. (5) and implies that there is a direct correlation between D and T_c over the entire temperature range. In the present series of amorphous alloys, the spin-wave stiffness constant renormalizes with temperature in accordance with the comparison predicted by both localized (Heisenberg) model and itinerant model. However, the linear relation between D and T_c observed in the present work can be explained within the framework of two different models: the collective-electron model and the nearest-neighbor Heisenberg model.[50] According to the collective-electron model the value of T_c determined by SP excitations alone is defined as in the following equation:

$$D = mT_c, \tag{16}$$

where $m = (k_B/8.484k_F^2)$ and k_F is the Fermi radius. Equation (16) provides the slope as 0.014 meV Å^2 K^{-1}, when the value of $k_F = 1.5$ Å^2 is used. It is clear from the above equation that the relation between D and T_c should be a straight line, which passes through the origin. However, the slope obtained from Fig. 15 is one order of magnitude greater than that observed by this model. According to nearest-neighbor Heisenberg model, the slope m is defined as $k_B a^2/2(S+1)$,

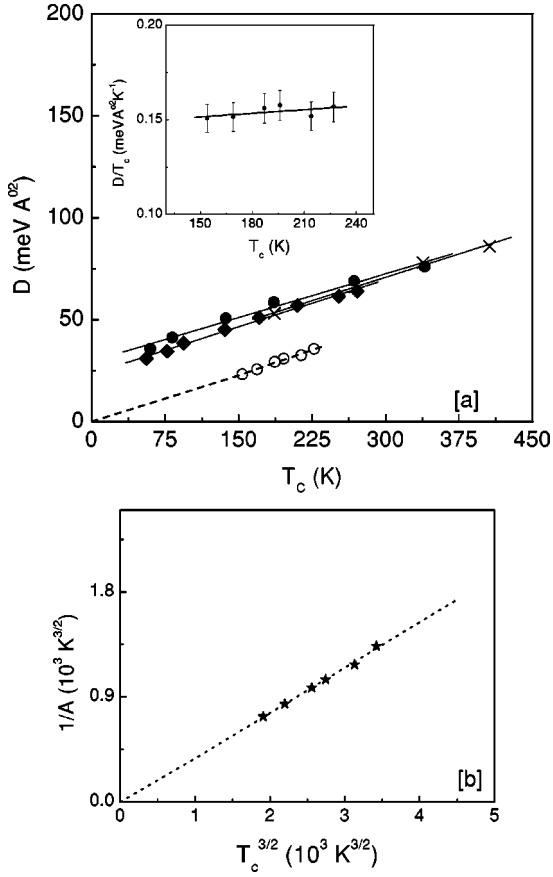

FIG. 15. (a) The spin-wave stiffness constant is plotted against Curie temperature. The dashed line passing through the data points is the best fit obtained by Eq. (16). Note: The value of D extracted from the other $[(Fe_xNi_{1-x})_{80}(B,Si)_{20}$ and $(Fe_xNi_{1-x})_{80}(P,B)_{20}]$ systems (Ref. 48) is also shown for comparison. Inset: the ratio between D and T_c is plotted against T_c. (b) the inverse of coefficient of $T^{3/2}$ term is plotted against $T_c^{3/2}$. The dotted line passing through data points shows the best fit.

where a is the nearest-neighbor distance and S is the localized atomic spin. However, Eq. (16) gives the slope values of 0.140 and 0.187 meV Å^2 K^{-1} for $S=1$ and $S=1/2$, respectively, using the value of nearest-neighbor distance[51] $a=2.55$ Å. This is in excellent quantitative agreement with the experimentally observed slope $m=D/T_c=0.1449$ meV Å^2 K^{-1} for this system. The calculated value of nearest-neighbor distance is 2.57 ± 0.04 Å, which is close to the values predicted for typical mean nearest neighbor TM-TM distances in amorphous ferromagnets.[51] Within the framework of Heisenberg model, Krey[52] has shown that T_c decreases and the constant $A(B)$ shows a weak (very weak) increasing trend. The temperature range over which $(T/T_c)^{3/2}$ term dominates become wider. The coefficient $A(B)$ shows the weak (very weak) dependence on Mn concentration compared to other amorphous systems. The SW excitation constant calculated on similar systems[26] shows very little variation with Mn concentration. This may be due to the fact that the analysis was done by neglecting the contribution from SP excitations. As shown from the present analysis, the SW excitations and SP excitations plus local-spin-density fluctuations[31] are dominant in the temperature ranges $0.16T_c\leqslant T\leqslant 0.40T_c$ and $0.42T_c\leqslant T\leqslant 0.88T_c$, respectively. However, the local-spin-density fluctuations are strongly suppressed by the external field and hence the temperature dependence of the in-field magnetization is solely governed by the SW and SP excitations for temperatures up to $0.9T_c$. For temperatures above and below this range $(0.9T_c<T<1.2T_c)$ the fit deviates considerably from the experimental data due to enhanced fluctuations in the magnetization[31] for temperatures close to T_c and the contribution from excitations is much less at low temperatures.

Within the framework of the band model, the effect of increasing the Mn concentration should decrease the exchange splitting ($\Delta E=I\sigma_s/N\mu_B$, where N is the number of spins per unit volume and I is the Stoner parameter) of spin-up and spin-down d subbands and shifts the Fermi level (E_F) to lower energies (as the spontaneous magnetization decreases with increasing x). In this context, the observation that the SW excitation alone seems to account for the observed thermal demagnetization of the spontaneous magnetization for temperature below a certain reduced temperature, which increases with x but the existence of an additional contribution from weak itinerant-type single-particle excitation cannot be ruled out. This implies that E_F lies within the $d_\downarrow$ and $d_\uparrow$ subbands in the entire composition range of the present study in contrast to the Co substituted samples. The effect of increasing field in the itinerant picture is to increase the splitting between the spin-up and spin-down subbands and hence by analogy to the influence of increasing ΔE by field, strongly suppressing the local spin-density fluctuations. This is in agreement with the results of the spontaneous resistive anisotropy[53] and high-field susceptibility of the same alloys.

The spontaneous magnetization does not go to zero at any temperature below T_c and the observation of a freezing temperature provides conclusive evidence for the existence of a *mixed phase* for $T<T_{sg}$. This is further supported from our ac susceptibility[28] measurements. There are two ways in which a substituting element can actively change the magnetization: these are (i) to change the Fe moment and (ii) to introduce the exchange frustration and drive the magnetic structure into collinear/noncollinear. Present analysis of the magnetization data indicates that the magnetic parameters obtained from this study, such as SG transition temperature, average magnetic moment, local magnetic anisotropy, coercive field, and large χ_{hf}, show systematic trends as a function of Mn concentration. Figure 16 shows a comparative study of magnetic parameters such as the average magnetic moment (μ_{ave}) and the χ_{hf} for various substituting elements as a function of concentration. The μ_{ave} is small for low Mn concentration compared to other substituting elements.[55] The μ_{ave} decreases monotonically with Mn concentration, in contrast with the Co substitution. The present series of samples show that the value of χ_{hf} is high and increases with increasing Mn concentration. Interestingly, the χ_{hf} is found to be large compared to other TM substitution. On the other hand, with Co substitution on FeZr the χ_{hf} drops rapidly at initial stages and attains the constant value for larger x. This suggests that the Co substitution in FeZr base form more

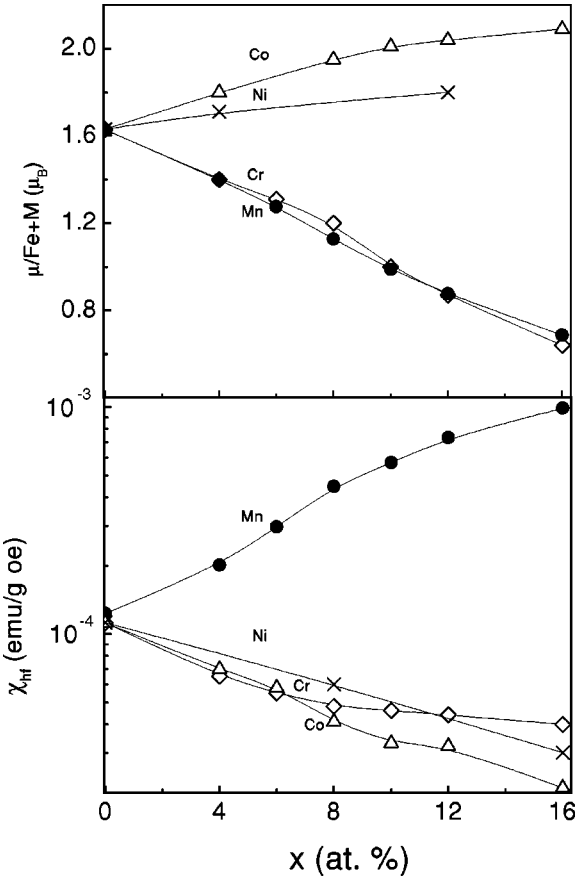

FIG. 16. (a) The average magnetic moment, (b) high-field susceptibility for amorphous $Fe_{90-x}M_xZr_{10}$ alloys as a function of M concentration x. Note that the values for Ni, Co, and Cr are extracted from Ref. 54.

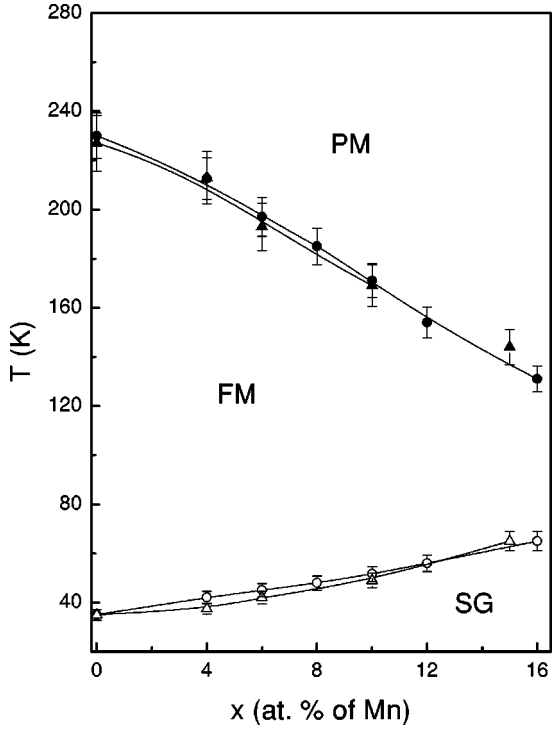

FIG. 17. The magnetic phase diagram for amorphous $Fe_{90-x}Mn_xZr_{10}$ alloys.

stable ferromagnetic alloy with its spin structure approaching the parallel alignment, which is consistent with the variation of other parameters such as T_c and μ_{ave}. Although the Cr substitution decreases the μ_{ave} that is similar to Mn substitution, the χ_{hf} is very low and comparable to that of Co and Ni substitution. Moreover, the reentrant behavior is not observed in Cr substituted samples. This indicates that the magnetism in Mn substituted samples is much more complicated compared to other TM substitutions and it could be speculated due to the frustration effects, which result in magnetic hardness as seen in Fig. 2. The large value of χ_{hf}, caused by flipping of weakly coupled antiferromagnetic (AFM) spins under high magnetic fields, is one characteristic feature of the invar effect. From the above discussion, it is tempting to suggest a possible existence of the noncollinear spin structure in the present series. Particularly, below T_c, the variation of χ_{hf} for all samples of present study shows a typical characteristic of the weak-itinerant ferromagnets.

In view of the exchange frustration model, the presence of FM and AFM exchange interactions in Mn substituted a-FeZr alloys can result either bond or site frustration or both. The sensitivity of the direct Fe-Fe exchange interaction to the distance between Fe-Fe atoms can be found from coordination numbers, which is 12 for AFM fcc Fe. Amorphous $Fe_{90}Zr_{10}$ alloys[56] have an average coordination number of 12–13, which supports the assumption of the presence of AFM exchange interactions. Three-dimensional Heisenberg Monte Carlo simulations with exchange frustration[57] indicate the development of double magnetic transition behavior as soon as the AFM interactions are present. However, the replacement of Fe by a small amount of Mn leads to a decrease in the number of Fe-Fe pairs,[58] but the substitution of Mn forms an AFM coupling between Fe and Mn (though the AFM coupling between Fe-Mn is weaker than the Fe-Fe coupling), which has a tendency to reduce the magnetic moment and Curie temperature, as we have observed in the present investigation. Recent Mossbauer studies also indicate the development of a low-field peak in the hyperfine field distribution as Mn concentration increased and this is attributed to an increase in AFM coupling.[26] This phenomenon, however, makes it difficult to interpret the observed results by the homogeneous exchange frustration model,[59] where the decrease of the magnetic order-disorder phase-transition temperature is due mainly to a reduction in the ferromagnetic interaction strength. Therefore we believe that in-field muon spin rotation (μSR) and Mossbauer measurements would throw some light on microscopic spin structure of the present system. Finally, the magnetic phase diagram of the amorphous $Fe_{90-x}Mn_xZr_{10}$ alloys is shown in Fig. 17. It is clear from the magnetic phase diagram that the multicritical point can be obtained at about 23 at.% of Mn. However, it is difficult to produce alloys with $x>16$ in amorphous form by the spin quenching technique.

V. CONCLUSION

We have analyzed in detail the critical behavior of a-$Fe_{90-x}Mn_xZr_{10}$ ($x=0-12$) alloys in the critical region

based on different methods using thermoremanent and thermomagnetization data as a function of temperature. The observed values of critical exponents are not a function of Mn content but are rather dependent on the temperature range of the data in the critical region selected for fitting procedure. Consistent with the Harris criterion the critical exponents are close to the Heisenberg values, which contradicts earlier analysis.[21] A combination of both spin-wave and single-particle excitations are essential to describe the thermomagnetization curve over a wide range of temperature ($T_{sg}<T<T_c$). The obtained results provide an evidence for *weak itinerant* ferromagnetic behavior in the present series of samples. The detailed analysis of magnetization data and the magnetic parameters obtained from the data indicates that the AFM coupling increases significantly as Mn concentration is increased, resulting in a greater degree of frustration that is consistent with the coexistence of FM and AFM states.

ACKNOWLEDGMENTS

One of the authors (A. Perumal) would like to thank the Council of Scientific and Industrial Research (CSIR), New Delhi, India, for providing financial support for this work. Research at Korea was supported by Korean Research Foundation Grant (KRF-99-005-D00038). Work conducted at Dalhousie University was funded by the Natural Sciences and Engineering Research Council of Canada.

*Corresponding author. Fax: 91-3222-55303; Email address: veeturi@phy.iitkgp.ernet.in

[1] Y. Kakehashi, Phys. Rev. B **41**, 9207 (1990); **43**, 10 820 (1991).
[2] S.N. Kaul, J. Phys.: Condens. Matter **3**, 4027 (1991).
[3] A. Perumal, V. Srinivas, V.V. Rao, and R.A. Dunlap, Physica B **292**, 164 (2000).
[4] A. Perumal, Pramana, J. Phys. **56**, 569 (2001).
[5] A.B. Harris, J. Phys. C **7**, 1671 (1974).
[6] H. Yamauchi, H. Onodora, and H. Yamamoto, J. Phys. Soc. Jpn. **53**, 747 (1984).
[7] S.N. Kaul, J. Phys. F: Met. Phys. **18**, 2089 (1988).
[8] D. Kaptas, T. Kemeny, L.F. Kiss, J. Balogh, L. Granasy, and I. Vincze, Phys. Rev. B **46**, 6600 (1992); N. Hegman, L.F. Kiss, and T. Kemeny, J. Phys.: Condens. Matter **6**, L427 (1994); I. Vincze, D. Kaptas, T. Kemeny, L.F. Kiss, and J. Balogh, Phys. Rev. Lett. **73**, 496 (1994).
[9] H. Yamamoto, H. Onodora, K. Hosoyama, T. Masumoto, and H. Yamauchi, J. Magn. Magn. Mater. **31-34**, 1579 (1983).
[10] D. Sherrington and S. Kirkpatrick, Phys. Rev. Lett. **35**, 1972 (1975).
[11] M. Gabay and G. Toulouse, Phys. Rev. Lett. **47**, 201 (1981).
[12] H. Hiroyoshi and K. Fukamichi, J. Appl. Phys. **53**, 2226 (1982).
[13] D.A. Read, T. Moyo, and G.C. Hallam, J. Magn. Magn. Mater. **44**, 279 (1984); D.A. Read, G.C. Hallam, and M. Chirwa, *ibid.* **82**, 83 (1989).
[14] D.H. Ryan, J.M.D. Coey, E. Batalla, Z. Altounian, and J.O. Strom-Olsen, Phys. Rev. B **35**, 8630 (1987); D.H. Ryan, J.O. Strom-Olsen, R. Provencher, and M. Townsend, J. Appl. Phys. **64**, 5787 (1988); M. Ghafari, W. Keune, R.A. Brand, R.K. Day, and J.B. Dunlap, Mater. Sci. Eng. **99**, 65 (1988); M. Ghafari, M. Chmielek, W. Keune, and C.P. Foley, Physica B **161**, 222 (1989); D.H. Ryan and H. Ren, J. Appl. Phys. **69**, 5057 (1991); D.H. Ryan, J. VanLierop, M.E. Pumarol, M. Roseman, and J.M. Cadogen, Phys. Rev. B **63**, 140405 (2001).
[15] S.N. Kaul, IEEE Trans. Magn. **MAG-20**, 1290 (1984); S.N. Kaul, J. Magn. Magn. Mater. **53**, 5 (1986); S.N. Kaul, J. Appl. Phys. **61**, 451 (1987); S.N. Kaul, C. Bansal, T. Kumaran, and M. Havalgi, Phys. Rev. B **38**, 9248 (1988); S.N. Kaul and V. Siruguri, J. Phys.: Condens. Matter **4**, 505 (1991); S.N. Kaul, V. Siruguri, and G. Chandra, Phys. Rev. B **45**, 12 343 (1992).
[16] K. Winschuh and M. Rosenberg, J. Appl. Phys. **61**, 4401 (1987).
[17] B.G. Shen, W. Yi-zhong, C. Jin-chang, Jian-gao Zhao, and Z. Wen-Zhan, J. Phys. C **8**, 1161 (1988).
[18] M. Ghafari, W. Keune, N. Chmielek, R.A. Brand, M.F. Braun, and M. Maurer, J. Phys. C **8**, 1145 (1988).
[19] B.G. Shen, Z. Zhiying, G.U. Benzi, Guo Huiqun, and Z. Jiangao, Chin. Phys. Lett. **6**, 522 (1989).
[20] B.G. Shen, G.U. Benxi, Z. Zhiying, Guo Huiqun, and Z. Jiangao, Chin. Phys. Lett. **11**, 22 (1989).
[21] G.K. Nicolaides, G.C. Hadjipanayis, and K.V. Rao, Phys. Rev. B **48**, 12 759 (1993).
[22] P.D. Babu and S.N. Kaul, Phys. Rev. B **52**, 10 637 (1995).
[23] P.L. Paulose and V. Nagarajan, Phys. Rev. B **54**, 14 934 (1996); D.H. Ryan, J.M. Cadogen, and J.Van Lierop, *ibid.* **62**, 8638 (2000).
[24] P.D. Babu and S.N. Kaul, J. Phys.: Condens. Matter **9**, 3625 (1997).
[25] P.D. Babu and S.N. Kaul, J. Phys.: Condens. Matter **9**, 7189 (1997).
[26] P.L. Paulose, S. Bhattacharya, V. Nagarajan, and R. Nagarajan, Solid State Commun. **104**, 767 (1997).
[27] M. Kopcewicz, A. Grabias, and B. Kopcewicz, J. Magn. Magn. Mater. **177-181**, 73 (1998).
[28] A. Perumal, V. Srinivas, V.V. Rao, and R.A. Dunlap, Phys. Status Solidi A **178**, 783 (2000).
[29] A. Perumal, V. Srinivas, V.V. Rao, and R.A. Dunlap, Mater. Sci. Eng., A **304-306**, 1004 (2001).
[30] A. Perumal, K.S. Kim, V. Srinivas, V.V. Rao, R.A. Dunlap, and S.C. Yu, J. Magn. Magn. Mater. **233**, 280 (2001).
[31] A. Perumal, K.S. Kim, S.C. Yu, V. Srinivas, V.V. Rao, and R.A. Dunlap, J. Magn. Magn. Mater. **226-230**, 1329 (2001).
[32] D.H. Ryan and J.M. Cadogan, J. Magn. Magn. Mater. **213**, 111 (2000); D.H. Ryan, J.M. Cadogan, and J.Van Lierop, J. Appl. Phys. **87**, 6525 (2000).
[33] A. Perumal, V. Srinivas, V.V. Rao, and R.A. Dunlap (unpublished).
[34] H. Hiroyoshi and K. Fukamichi, J. Appl. Phys. **53**, 2226 (1982).
[35] J.R.L. de Almeida and D.J. Thouless, J. Phys. **11**, 983 (1978).
[36] T.K. Nath, N. Sudhakar, E.J. McNiff, and A.K. Majumdar, Phys. Rev. B **55**, 12 389 (1997).
[37] S.N. Kaul, Phys. Rev. B **27**, 5761 (1982).
[38] F. Semadeni, B. Roessli, P. Boni, P. Vorderwisch, and T. Chatterji, Phys. Rev. B **62**, 1083 (2000).
[39] A.Z. Men'shikov, N.N. Kuz'min, V.A. Kazantsev, S.N. Sidorov, and V.N. Kalinin, Phys. Met. Metallogr. **40**, 174 (1975).

[40] B.E. Argyle, S.H. Charap, and E.W. Push, Phys. Rev. B **2**, 2051 (1963).
[41] C. Herring in *Magnetism*, edited by G.T. Rade and H. Suhl (Academic Press, New York, 1966), Vol. IV.
[42] W. Marshell and S.W. Lovesey, *Theory of Thermal Neutron Scattering* (Oxford University Press, New York, 1971).
[43] K.S. Kim, S.C. Yu, A. Perumal, V. Srinivas, V.V. Rao, and R.A. Dunlap, in *Joint Intermag MMM Conference*, January 7-11, 2001, San Antonio, Texas.
[44] J.E. Noakes and A. Arrott, J. Appl. Phys. **38**, 973 (1967).
[45] T. Mizoguchi and K. Yamauchi, J. Phys. (Paris) **35**, C4-287 (1974); K. Yamada, Y. Ihikawa, J. Endo, and T. Masumoto, Solid State Commun. **16**, 1335 (1975); Z. Marohnic, D. Drobac, E. Babic, and K. Zardo, J. Magn. Magn. Mater. **38**, 93 (1983).
[46] J.S. Kouvel and M.E. Fisher, Phys. Rev. B **136**, 1626 (1964).
[47] M. Fahnle, P. Broun, R. Reisser, M. Seeger, and H. Kronmuller, J. Phys. C **8**, 1201 (1988); P.D. Babu and S.N. Kaul, Phys. Rev. B **52**, 10 637 (1995).
[48] S.N. Kaul and P.D. Babu, Phys. Rev. B **50**, 9308 (1994); S.N. Kaul and P.D. Babu, J. Phys.: Condens. Matter **4**, 6429 (1992); S.N. Kaul, Phys. Rev. B **27**, 5761 (1983).
[49] A. Perumal, Ph.D. thesis, submitted to IIT-Kharagpur, India, 2001.
[50] A. Katsuki and E.P. Wohlfarth, Proc. R. Soc. London, Ser. A **295**, 182 (1966).
[51] G.S. Cargill III, in Solid State Physics, edited by H. Ehrenrich, F. Seitz, and D. Turnbill (Academic, New York, 1975), Vol. 30, p. 227.
[52] U. Krey, Z. Phys. B **31**, 247 (1978).
[53] A. Perumal, V. Srinivas, V.V. Rao, and R.A. Dunlap (unpublished).
[54] Shen Bao-gen, Xu Ruferg, Zhao Jian-gao, and Zhan Wen-Shan, Phys. Rev. B **43**, 11 005 (1991).
[55] Shen Bao-gen, Zhan Wen-Shan, Zhao Jian-Gao, and Chen Jin-Chang, Acta Phys. Sin. **34**, 1009 (1985); Zhan Wen Shan, Shen Bao-gen, and Zhao Jian-gao, *ibid.* **34**, 1613 (1985).
[56] H.S. Chen, K.T. Aust, and Y. Waseda, J. Non-Cryst. Solids **46**, 307 (1981).
[57] J.R. Thomson, Guo Hong, D.H. Ryan, M.J. Zuckermann, and M. Grant, Phys. Rev. B **45**, 3129 (1992); J.R. Thomson, Guo Hong, D.H. Ryan, M.J. Zuckermann, and M. Grant, J. Appl. Phys. **69**, 5231 (1991).
[58] P.L. Paulose, S. Bhattacharya, and V. Nagarajan, J. Appl. Phys. **81**, 5282 (1997).
[59] Hong Ren and D.H. Ryan, Phys. Rev. B **51**, 15 885 (1995).